Improved Modeling for the Reheat Phase in Thermoforming Through an Uncertainty Treatment of the Key Parameters

A. YOUSEFI, A. BENDADA, *and* R. DIRADDO

Industrial Materials Institute
National Research Council of Canada
75 De Mortagne Blvd.
Boucherville, Quebec, J4B 6Y4 Canada

This work focuses on the treatment of parameter uncertainty in the simulation of the sheet reheat phase of the thermoforming process. The approach aims to improve the quality of predictions through more accurate evaluation of the input parameters. First, the modeling approach is employed to perform a sensitivity analysis on the reheat phase. Then, a series of specialized experiments with heat flux and temperature sensors are performed on a thermoforming machine. The key parameters identified through the sensitivity analysis are the subject of these experiments. The natural convective heat transfer coefficients are evaluated by two different approaches. Through treatment of the uncertainty associated with the input parameters, the prediction of sheet reheat phase is significantly improved.

INTRODUCTION

The thermoforming process involves three stages: sheet reheat, forming, and solidification. A polymeric sheet is heated in an oven to the desired forming temperature distribution. The sheet is then deformed to take the shape of the mold cavity and subsequently solidified.

Process modeling is a useful tool in reducing the process set-up times and tooling costs and in achieving the desired product development goals. Accurate prediction of sheet reheat in thermoforming process is critical as it is the input for the highly temperature dependent forming simulation. Therefore, accurate prediction of the temperature is essential to obtain an accurate prediction of the final part thickness. Process simulation traditionally relies on the exact knowledge of parameter inputs, such as material properties, process conditions and heat transfer properties. However, these parameters are never known exactly, and a degree of uncertainty exists. The uncertainty directly affects the confidence in the results obtained. One therefore has two options—reduce the level of uncertainty or account for it in the simulation through appropriate sensitivity treatment.

Heating thermoplastics has been the subject of some research works in the literature. Gross (1) summarized the methods of analyzing the heating processes for thermoplastics. He discussed various mechanisms of heat transport for a variety of polymers processing techniques. Throne (2) discussed various aspects of computer-aided design in thermoforming. The sheet heating was characterized through assigning approximate values to the processing parameters involved in the reheat phase. In another work, Throne (3) also analyzed modeling of heat transfer in semitransparent polymers for thermoforming applications by addressing the wavelength dependency of sheet absorptivity and heater emissivity. Schmidt *et al.* (4) underlined the importance of optimizing the reheating stage in blow molding and thermoforming. They predicted the transient temperature distributions for both thin and thick-gage polypropylene thermoformed sheets using a radiative heat transfer analysis. An effective radiative heat transfer coefficient and the effective bulk temperature were used for this analysis. Monteix (5) optimized the set of processing parameters for the reheat phase of 2-stage injection stretch blow molding process. The optimization task included the measurement of oven air temperature as well as the evaluation of heat transfer coefficients at the surface of PET preforms and sheets. Le Maoult *et al.* (6) and Monteix *et al.* (7) determined the spectral properties of infrared emitters. Bendada *et al.* (8) developed an inverse technique to reconstruct the initial temperature profile in a preform as well as the free convection coefficient using surface temperature measurements. In a recent work, Haberstroh *et al.* (9) have analyzed the mobile

preform reheat in injection stretch blow molding process. There are also some other works in the literature on the simulation of reheat phase for forming processes (10–14); however, the effect of process variables on the reheat stage has not been addressed in details. To the authors' knowledge, this is the first work to deal with the sheet reheat stage in details. Moreover, the new methodology developed in this work is the first attempt to remove uncertainties associated with the input parameters in predicting the sheet temperature distribution.

This work focuses on the treatment of parameter uncertainty in the simulation of the sheet reheat phase of the thermoforming process. As the reheat phase is the first phase of the thermoforming process, errors in the prediction of this phase will be compounded in the prediction of subsequent phases. Furthermore, there are several parameters important to the prediction of the reheat phase that have a high degree of uncertainty. The approach aims to improve the quality of predictions through more accurate evaluation of the input parameters. First, the modeling approach is employed to perform a sensitivity analysis on the reheat phase. A single parameter at a time is perturbed in a fashion so as to determine the effects on the transient response of the sheet surface temperature. Then, a series of specialized experiments with heat flux and temperature sensors are performed on a thermoforming machine. The key parameters identified through the sensitivity analysis are the subject of these experiments. The natural convective heat transfer coefficients are evaluated by two different approaches. Through treatment of the uncertainty associated with the input parameters, the prediction of sheet reheat phase is significantly improved.

THEORY

Proper simulation of the sheet reheat stage combines the heat transfer and viscoelastic deformations. The heat transfer analysis couples radiation and convection boundary conditions on both sides of the sheet. A non-isothermal viscoelastic formulation is used to represent the sheet deformation due to a gravity load or an applied pressure. Therefore the thermal and sag predictions are coupled in the reheat stage.

If a temperature gradient exists within a body, heat is transported from the area of higher temperature to that of lower temperature. If an energy balance is set up for a volume element where the thickness is much lower than the other two dimensions, then one obtains the differential equation for the temperature field as follows (15):

$$\rho C_p \frac{\partial T}{\partial t} = k\frac{\partial^2 T}{\partial x^2} + \frac{\partial \dot{q}_{abs}}{\partial x} \tag{1}$$

where ρ, C_p, and k are the density, specific heat and thermal conductivity of the body, respectively, T is the temperature, x is the coordinate of the sheet in the thickness direction, and t is the elapsed time. The last term in the right hand side, $\frac{\partial \dot{q}_{abs}}{\partial x}$ is taken into consideration when there is heat absorption in the volume from a radiative heat source. In radiative heating of opaque materials, the volume heat absorption term is considered to be negligible. It is important to note that the presence of clamp frame introduces an important temperature gradient in the planar direction, which is neglected in one-dimensional modeling of the sheet reheat phase.

The heat balance equation is subjected to a series of boundary conditions. For the radiative heating stage in thermoforming, one is dealing with both radiative and convective boundary conditions. As a consequence, the simulation of the reheat stage requires accurate modeling of the heat flux received by the polymer sheet. The total heat flux $\dot{q}_{tot}$ at the sheet surface is given by:

$$\dot{q}_{tot} = \dot{q}_{rad} + \dot{q}_{conv} \tag{2}$$

where

$$\dot{q}_{rad} = \sigma \varepsilon_{eff} F(T_h^4 - T_s^4) \tag{3}$$

and

$$\dot{q}_{conv} = h(T_\infty - T_s) \tag{4}$$

In these equations, $\dot{q}_{rad}$ is the radiative heat flux incident on the surface, $\dot{q}_{conv}$ is the convective heat flux, σ is the Stefan-Boltzmann constant, F is the view factor, T_h is the heater temperature, T_s is the sheet surface temperature, h is the natural convective heat transfer coefficient, T_∞ is the air temperature, and ε_{eff} is the effective emissivity of the sheet-heater system defined as (16):

$$\varepsilon_{eff} = \left[\frac{1}{\varepsilon_h} + \frac{1}{\varepsilon_s} - 1\right]^{-1} \tag{5}$$

where ε_h and ε_s are the emissivities for the heater and the sheet, respectively. The incident radiant heat is absorbed, reflected or transmitted depending on the material under consideration. Since the ABS sheets used in this work are opaque and adequately thick (1.6 mm), the radiation is assumed to be fully absorbed on the surface.

To calculate the radiative heat flux incident on the sheet surface, the oven is modeled with triangular elements representing the zone surfaces. The global radiative heat flux received by the sheet becomes the summation of each heater element contribution according to the following equation (17):

$$\dot{q}_{rad} = \sum_i \sigma \varepsilon_{eff,i} A_i F_{ij} (T_i^4 - T_s^4) \tag{6}$$

where A_i is the individual source element surface area, F_{ij} is the view factor between i^{th} element of the source and j^{th} element of the sheet, and T_i is the source element temperature. Radiative exchanges with other oven components are neglected. The view factor, F_{ij}, is evaluated as follows:

$$F_{ij} = \frac{1}{\pi A_i}\Sigma_i \Sigma_j \frac{\cos\theta_i \cos\theta_j}{d^2} A_i A_j \quad (7)$$

where θ_i and θ_j are the direction cosines on i^{th} element of the source and j^{th} element of the sheet, respectively, d is the distance between these elements, and A_i and A_j are their respective surface area.

The sheet sag as well as the sheet forming is predicted with the K-BKZ viscoelastic constitutive model. This model has shown to be capable of predicting the viscoelastic deformation of most thermoforming grade plastics during the forming processes including their deformation under the gravity load (10). The K-BKZ model relates the stress to the strain history as follows (18).

$$\boldsymbol{\sigma} = -q\boldsymbol{\delta} + \frac{1}{1-\theta}\int_{-\infty}^{t} m(t-\tau)h(I_1, I_2)(\mathbf{c}^{-1}(\tau, t) + \theta\mathbf{c}(\tau, t))d\tau \quad (8)$$

where q is the hydrostatic pressure, δ is the identity tensor, m is a memory function given by the Maxwell relaxation spectrum, $\mathbf{c}$ is the Cauchy deformation tensor, $\mathbf{c}^{-1}$ is the Finger deformation tensor, h is a damping function based on the Cauchy strain invariants and θ refers to the second normal stress difference in the deformation (biaxial effect).

The thermal dependence of the K-BKZ model is accounted for with a temperature shift function that modifies the modulus or the relaxation times of viscoelastic models. The most common shift function used is the WLF equation:

$$\ln(a_T) = -\frac{c_1 (T - T_{ref})}{c_2 + T - T_{ref}} \quad (9)$$

where c_1 and c_2 are model constants and T_{ref} is the reference temperature at which the shift a_T equals 1.

To theoretically evaluate the natural convective heat transfer coefficients, empirical equations are used. These equations are generally of the following form (19):

$$\overline{Nu_L} = \frac{\bar{h}L}{k} = CRa_L^n \quad (10)$$

where $\overline{Nu_L}$ is the average Nusselt number, $\bar{h}$ is the average heat transfer coefficient, k is the thermal conductivity of air, and C and n are constants. The Rayleigh number,

$$Ra_L = \frac{g\beta(T_s - T_\infty)L^3}{\nu\alpha} \quad (11)$$

is based on the characteristic length L of the geometry defined as follows:

$$L \equiv \frac{A_s}{P} \quad (12)$$

where A_s and P are the plate surface area and perimeter, respectively. In *Eq 11*, g is the local acceleration due to gravity, β is the thermal expansion coefficient, T_s is the plate surface temperature, T_∞ is the air temperature, ν is the kinematic viscosity and α is the thermal diffusivity of air.

The following equations give the heat transfer coefficients for the upper surface of a heated plate or the lower surface of a cooled plate:

$$\overline{Nu_L} = 0.54Ra_L^{1/4} \quad 10^4 \le Ra_L \le 10^7 \quad (13)$$

$$\overline{Nu_L} = 0.54Ra_L^{1/3} \quad 10^7 \le Ra_L \le 10^{11} \quad (14)$$

Similarly, the heat transfer coefficient for the lower surface of a heated plate or the upper surface of a cooled plate is:

$$\overline{Nu_L} = 0.27Ra_L^{1/4} \quad 10^5 \le Ra_L \le 10^{10} \quad (15)$$

This work aims to improve the quality of temperature predictions through more accurate evaluation of the input parameters. The parameters were selected based on either their major effect on the reheat phase or the uncertainty involved with their real values under processing conditions.

SENSITIVITY ANALYSIS

The modeling approach was employed to analyze the sensitivity of the sheet reheat phase to the key parameters of the thermoforming process. The sheet was meshed using 9360 triangular multilayer membrane elements and the simulations were performed using FormSim software (10, 20). The parameters were selected based on either their major effect on the reheat phase or the uncertainty involved with their real values under processing conditions. The parameters of interest were oven temperature, air temperature, emissivity, view factor, heat transfer coefficient, sheet specific heat, sheet thermal conductivity, and heater-sheet spacing. A single parameter at a time was perturbed in a fashion so as to determine the effects on the transient response of the sheet surface temperature. The procedure can be summarized as follows:

1. Perturb one parameter at a time (15%) and run the FormSim code to get the sheet surface temperature distribution
2. Track the surface temperature after 90, 120, 150, and 180 s reheat period and compare the simulation results with the control condition ($T_{control}$: reference temperature profile with no perturbation) along the transversal symmetry axis featuring the highest temperature gradient
3. Spot the perturbation for which the surface temperature is the highest along the symmetry axis and take the maximum temperature difference obtained (T_{max}–$T_{control}$) as the basis for normalization procedure
4. Plot the normalized sensitivity $(T-T_{control})/(T_{max}-T_{control})$ along the symmetry axis and, for the center of the sheet, as a function of reheat time for all perturbed cases

In this work, the normalized sensitivity results for the center of the sheet as a function of reheat time are presented.

EXPERIMENTAL

The experimental measurements were performed on an industrial scale thermoforming machine. The ABS sheet dimensions were 240-mm width, 252-mm length, and 1.6-mm thickness. The oven had an upper and a lower heater bank of six ceramic elements for profiled control of three zones. First, the ceramic heaters were calibrated at three different set points (dialed in temperatures). To this end, the surface temperatures of the heater banks were measured at different set points using mounted type K thermocouples. The average temperature of the coil and support on each heating element was found to represent best the heater temperature. The calibration curve was constructed by plotting the measured temperature *versus* set point temperature.

Figure 1 shows the experimental setup including the location of thermocouples measuring oven, sheet and air temperatures. For an oven set-point temperature of 180°C and 360-s reheat time, the transient sheet surface temperature was measured at three different locations (both upper and lower sides) using mounted type K thermocouples. The sheet upper surface temperature was also measured using an AGEMA 900LW infrared camera right after removing the sheet from the oven. The two temperature readings were fairly comparable (less than 5% discrepancy).

Black-painted BF-02 series sensors from Vatell Co. (polyimide, 10 mm by 10 mm by 0.2 mm), equipped with a type T thermocouple on the top surface were used for heat flux measurements. A single heat flux sensor at a time was attached to the center of the ABS sheet (either upper or lower surface) using a conductive adhesive pad provided by Vatell Co. The transient heat flux (convective + radiative) as well as the top surface temperature of the heat flux sensor was measured. It was noticed that the temperature readings of the type T thermocouple integrated to the top surface of the sensor corresponded well to the sheet surface temperature readings using mounted thermocouples (less than 5% discrepancy). This indicates that the heat flux sensor does not disturb the heat flow.

The transient air temperature was measured using type K thermocouples, midway between the heater and the ABS sheet. The spots where the air temperature measurements were performed correspond to

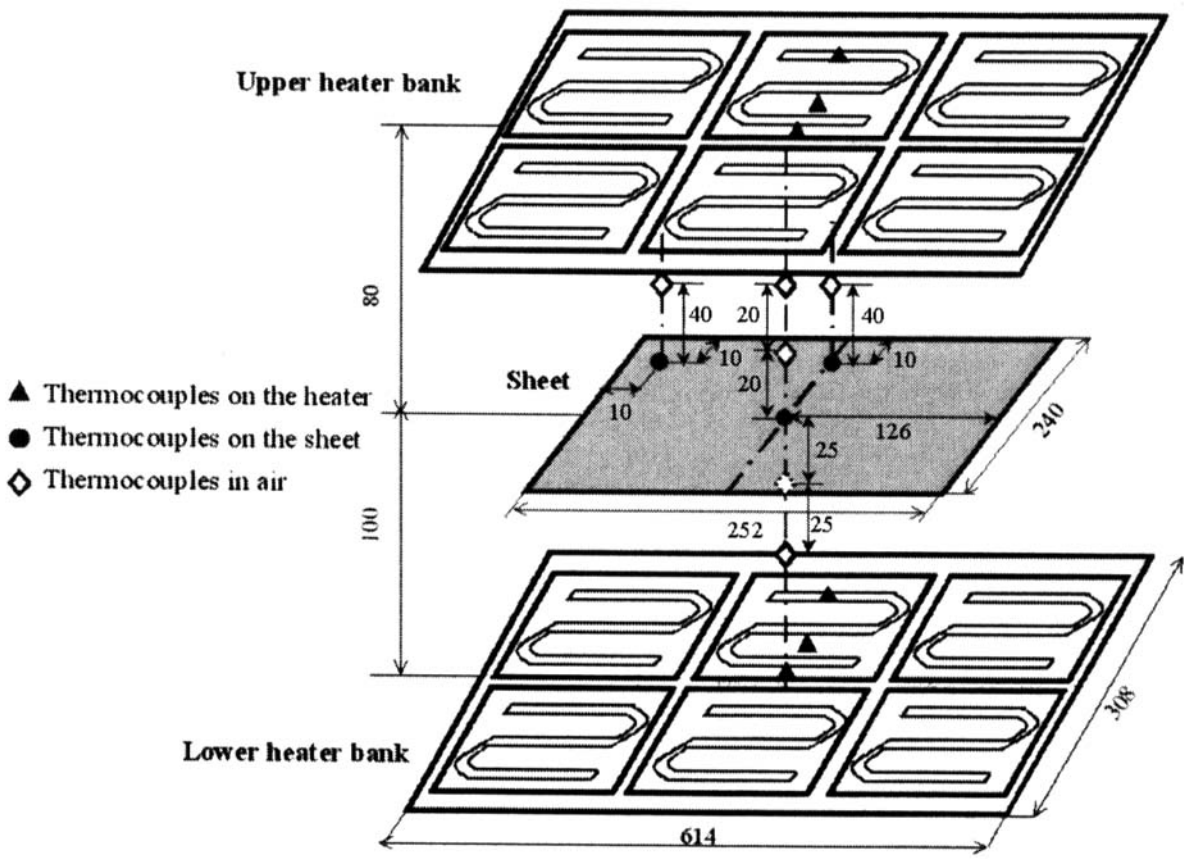

Fig. 1. Experimental setup including the location of thermocouples measuring the oven, sheet and air temperature. All dimensions are in mm.

those of sheet surface temperature measurements (see *Fig. 1*). The same procedure was repeated to measure the air temperature at several locations along the vertical symmetry axis.

The infrared camera was also used to measure the emissivity of the ABS sheet and ceramic heaters. A black paint of a known emissivity was applied to the test surface in order to create a reference value for the emissivity readings. The effective emissivity as a function of temperature was evaluated using *Eq 5*.

RESULTS AND DISCUSSION

Figure 2 compares the normalized sensitivity of the sheet surface temperature to the input parameters as functions of dimensionless heating time. Dimensionless scales allow a better demonstration of the relative effect of each parameter on the sheet surface temperature evolution and the time course during which these effects are significant. As a consequence these results are applicable to a wide range of thermoforming systems and materials. The results for thermal conductivity are not considered in this figure since it was found to have a little effect on the sheet surface temperature. However, for thick-gauge sheets, the effect of this parameter should be taken into consideration. These results indicate that the heater temperature, emissivity, view factor, and the polymer specific heat have the most pronounced effects among the parameters under investigation. Moreover, it can be seen that the sensitivity of the reheat phase to each parameter is dynamic in nature during reheat. While at the beginning of the reheat phase the specific heat and emissivity have pronounced effects, the heat transfer coefficient becomes more predominant towards the end of the reheat.

The sensitivity analysis indicates the influence of the input parameters on the reheat phase assuming the same level of uncertainty for each parameter. However, in practice the uncertainty varies from one parameter to another. The following results demonstrate the level of uncertainty for each parameter.

The temperature distribution histogram of the lower heater bank obtained using the infrared camera is shown in *Fig. 3*. Although the set-point is 180°C, about 9% of the surface falls below the set-point, representing the gap between the heating elements. Furthermore, over half the surface is at temperatures between 200°C and 220°C. Combining new and old heating elements can lead to this kind of temperature nonuniformity.

Figure 4 shows the transient temperature of the heater banks measured at a set-point of 180°C. A significant discrepancy is observed between the set-point and the measured temperatures for the upper heater bank, particularly toward the end of the reheat phase. Therefore, the heater temperatures input in the simulations must be time-dependent to properly predict the reheat stage. An alternative would be to obtain a better transient temperature control of the heating zones.

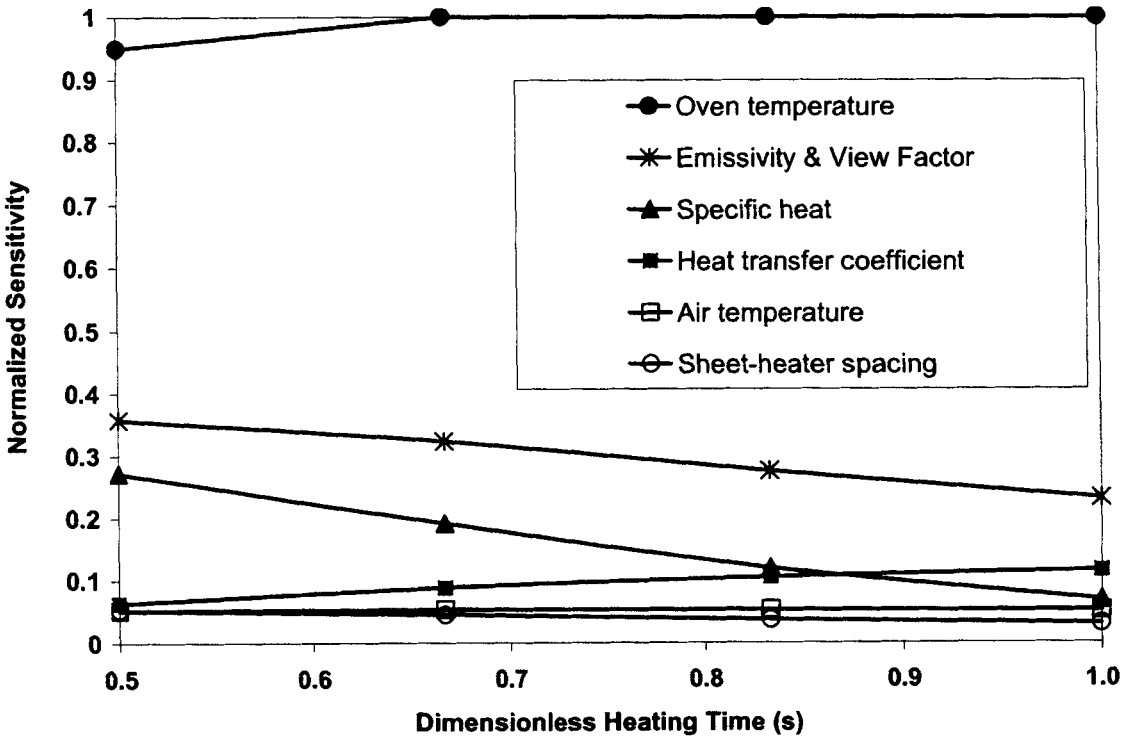

Fig. 2. Normalized sensitivity as a function of dimensionless heating time for some input parameters. The overall heating time is 180 s.

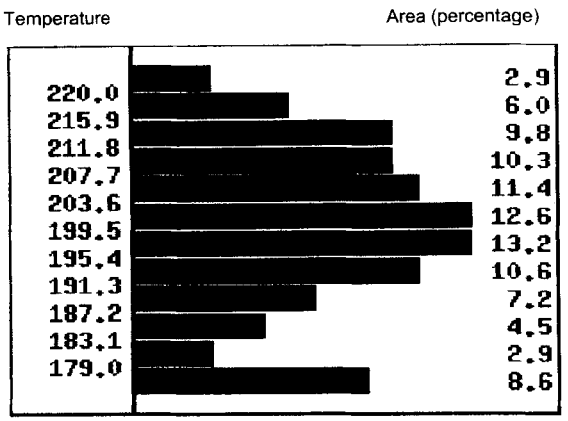

Fig. 3. Temperature distribution histogram giving the temperature vs. percentage of area for the lower heater bank.

The sheet surface temperatures measured at three different locations using both mounted thermocouples and the infrared camera are given in *Fig. 5*. As expected, the temperature is higher at the center and decreases towards the edges, with a minimum at the corners. This can be explained by the diminishing magnitude of the view factor towards the edges. The thermal conduction in the planar direction due to the presence of the clamp frame is also responsible in part for the observed temperature gradient. *Figure 5* also shows that the temperature is higher at the lower side of the sheet than at the upper side of the sheet due to rising hot air. The temperature reading using the infrared camera at the end of the reheat period is slightly higher at the edge. The lack of proper contact between the mounted thermocouple and the sheet could be responsible for this discrepancy.

Figures 6 to *8* show the air temperatures measured midway between the sheet and heater banks at the upper and lower side of the sheet as well as those measured along the vertical symmetry axis. The results imply that the oven air temperature is extremely nonuniform and changes significantly with heating time. Moreover, the air temperatures at the lower side of the sheet are 1.5 to 2 times greater that the values at the upper side. This can be attributed to the clamp frame at the lower side, which creates a stagnant region by trapping the hot air. The fluctuation in the temperature readings is probably due to the circulation of the oven air caused by natural heat convection phenomena. The following correlation was used to represent the air temperature as a function of reheat time (21):

$$T(t) = T_f + (T_i - T_f)e^{-bt} \tag{16}$$

where $T(t)$ is the transient air temperature, b is a parameter related to the heating rate, T_f is the final air temperatures at the end of reheat, and T_i is the initial air temperature related to the ambient temperature T_{amb} and oven temperature T_O as follows:

$$T_i = aT_o + (1 - a)T_{amb} \tag{17}$$

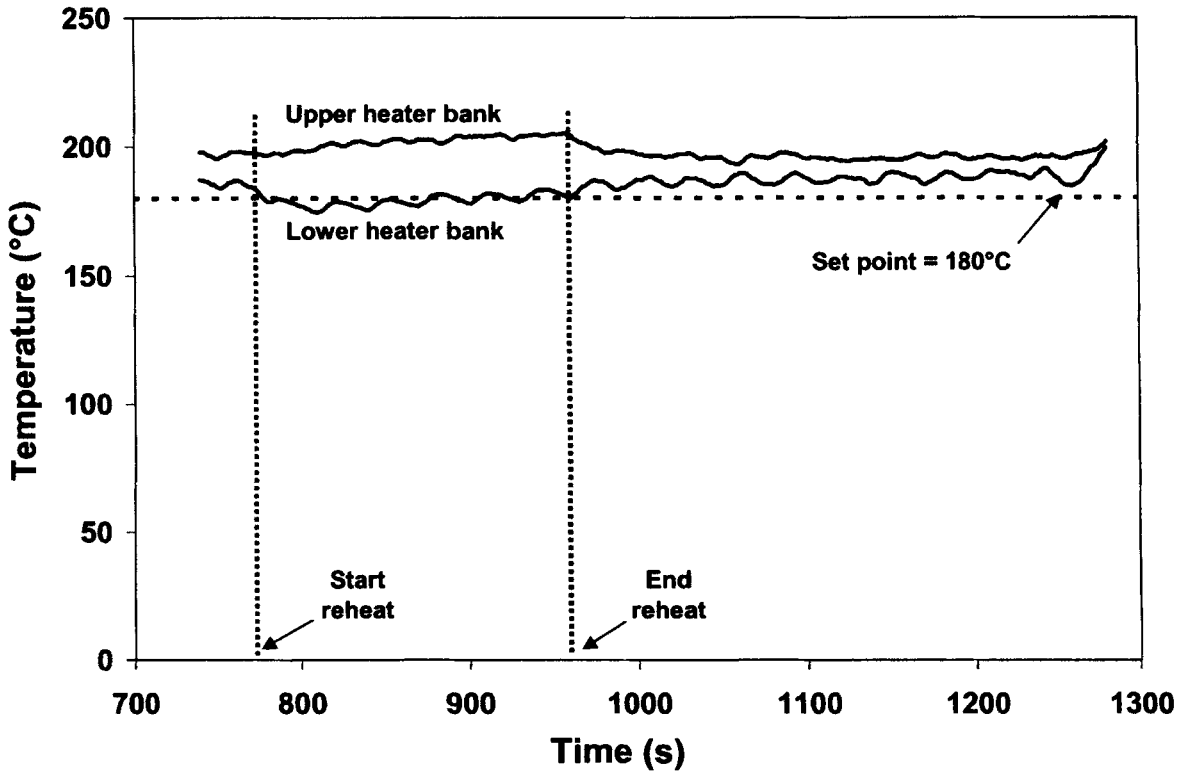

Fig. 4. Variations in the temperature of the heater banks vs. reheat time.

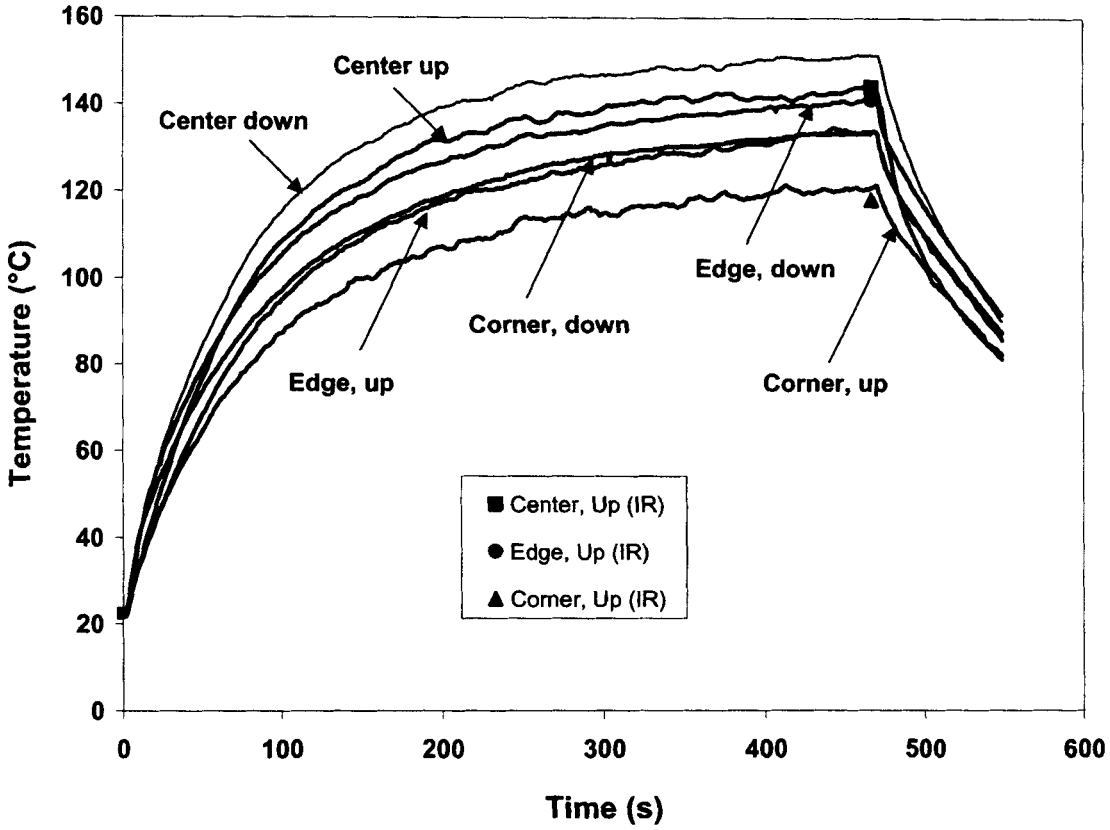

Fig. 5. Sheet surface temperatures measured at three different locations on the upper and the lower surface using both mounted thermocouples and infrared camera.

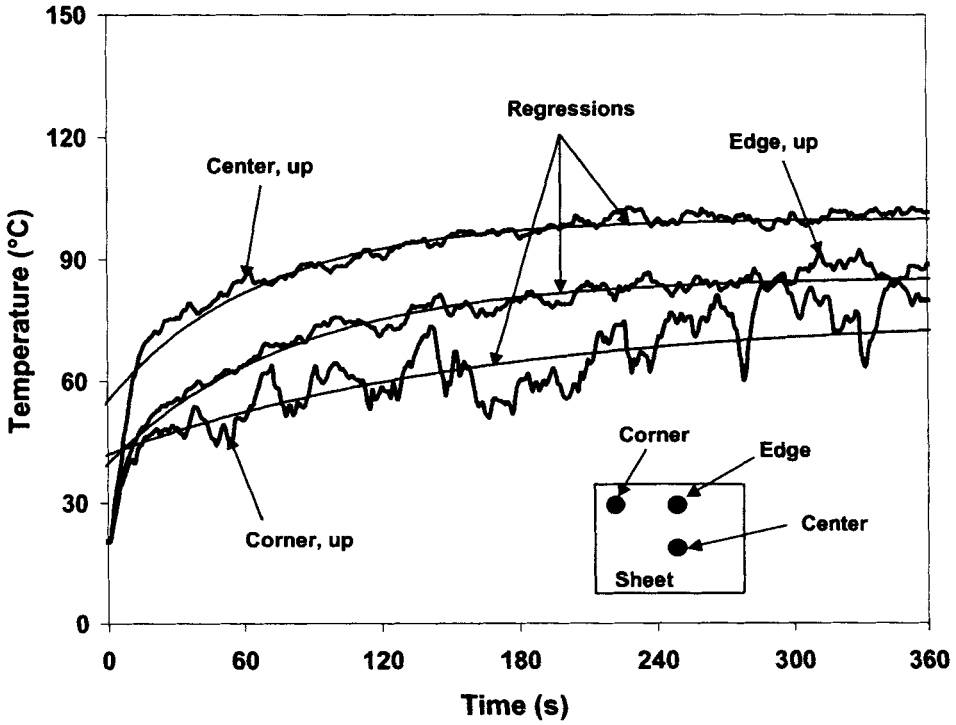

Fig. 6. Air temperature, measured midway between the sheet and upper heater bank.

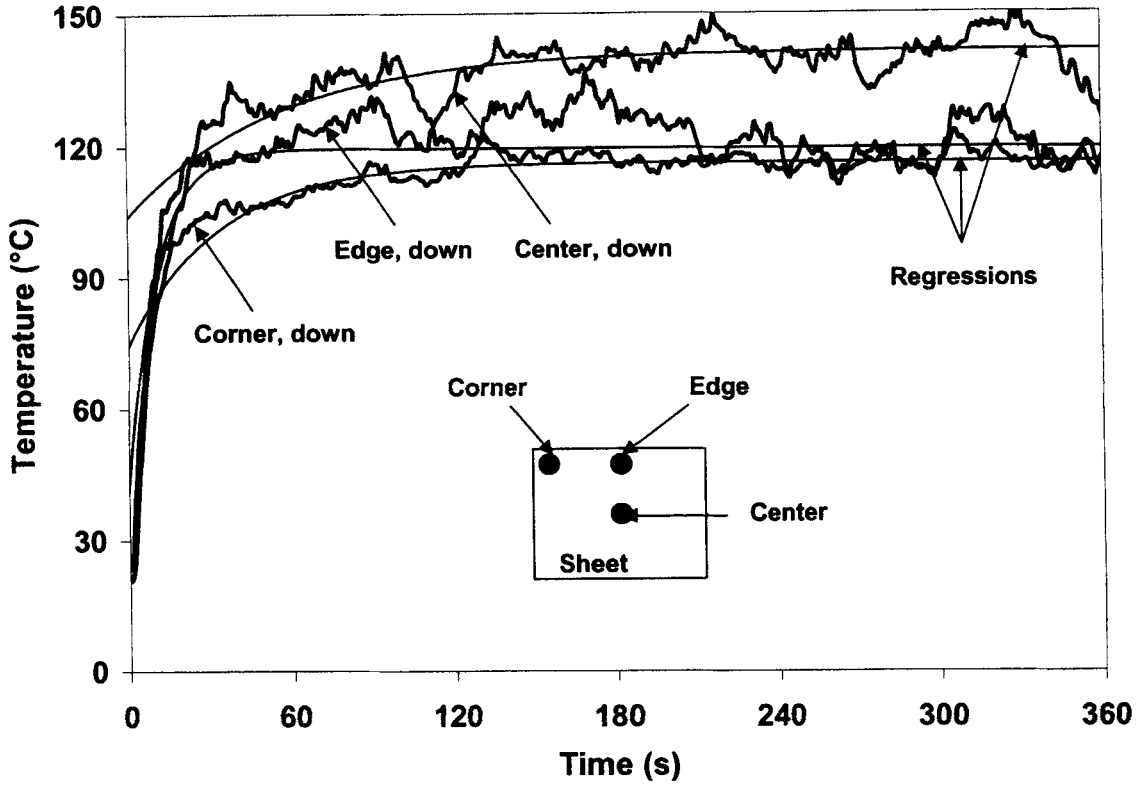

Fig. 7. Air temperature, measured midway between the sheet and lower heater bank.

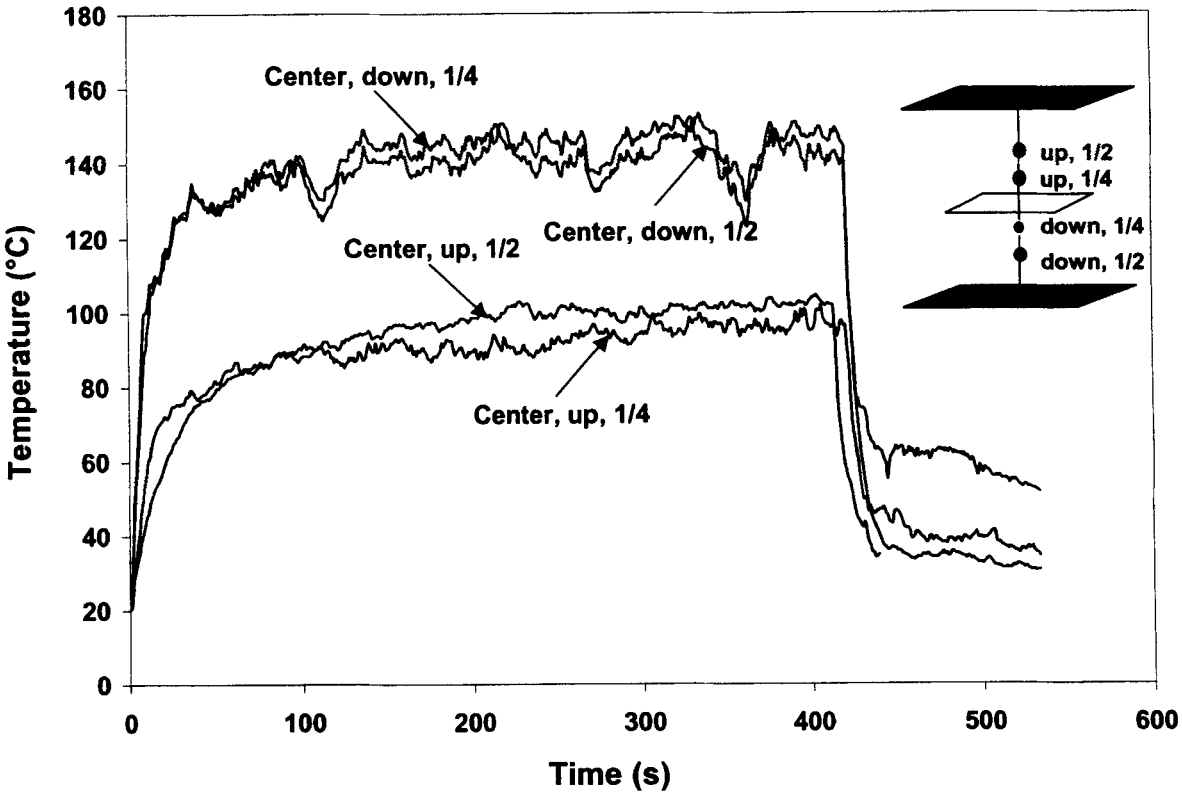

Fig. 8. Air temperature measured along vertical symmetry axis, between the heater banks and the ABS sheet.

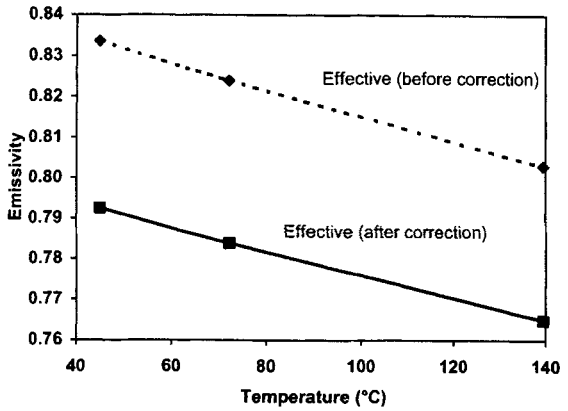

Fig. 9. Effective emissivity evaluated using Eq 5 before and after correction for the gap between the heating elements.

where a is a parameter below unity. The regression based on these equations is also shown in *Figs. 6* and *7*. Predicting the transient air temperature for various oven temperatures using *Eq 16* will be the subject of our future work. To achieve this goal, appropriate correlation must be found for each fitting parameter to represent their variations with oven temperature.

Figure 9 gives the effective emissivity evaluated using *Eq 5* based on the measured emissivity values. Having observed a linear temperature dependency for the emissivity of the ceramic heaters (ε_h), the effective emissivity at higher temperatures was approximated through extrapolating the effective emissivity curve (dotted line). On the other hand, the infrared thermography of the heater banks indicated that around 9% of the heater area fell below the set-point temperature, representing the gap between the heating elements. As a consequence, the effective emissivity curve was corrected to represent the actual heater. The resulting curve (solid line) is also shown in *Fig. 9*. The extrapolated effective emissivity curve leads to a value around 0.7 at a heater temperature of 200°C.

The heat flux measurements enabled us to approximate the natural convective heat transfer coefficients. According to *Eqs 2–4*, the heat transfer coefficient can be evaluated as follows:

$$h = \frac{\dot{q}_{tot} - \sigma\varepsilon_{eff}F(T_h^4 - T_s^4)}{(T_\infty - T_s)} \tag{18}$$

Sheet surface temperature and air temperature are known *a priori* based on the experimental measurements conducted in this work. The radiative heat flux is evaluated based on the parameters measured in this work for the infrared heaters. The view factor for the heat flux sensor is evaluated numerically based on *Eq 7* using our SheetMesh software (10, 22). *Figure 10* gives both the total heat flux and radiative heat flux. According to these results, the heat flux measurements leads to a heat transfer coefficient value of 2 $W.m^{-2}.K^{-1}$ for the lower side of the sheet at the beginning of the

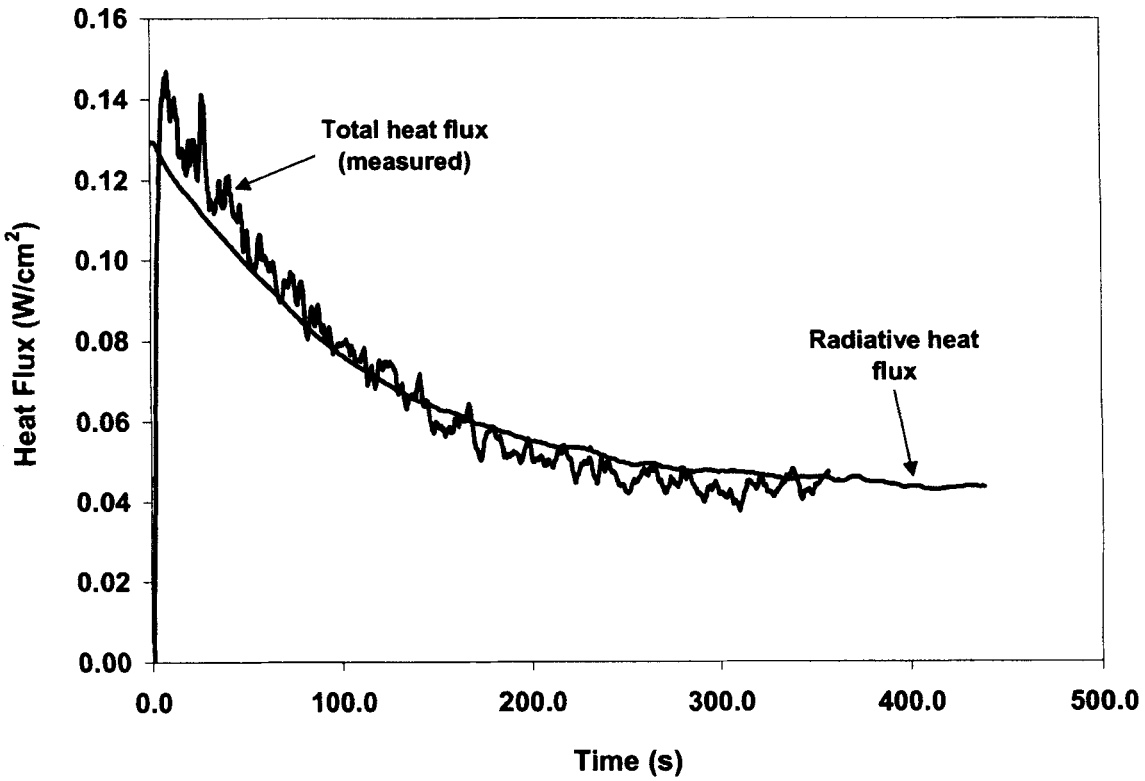

Fig. 10. Total heat flux (measured) and radiative heat flux (calculated) for the lower surface of the sheet.

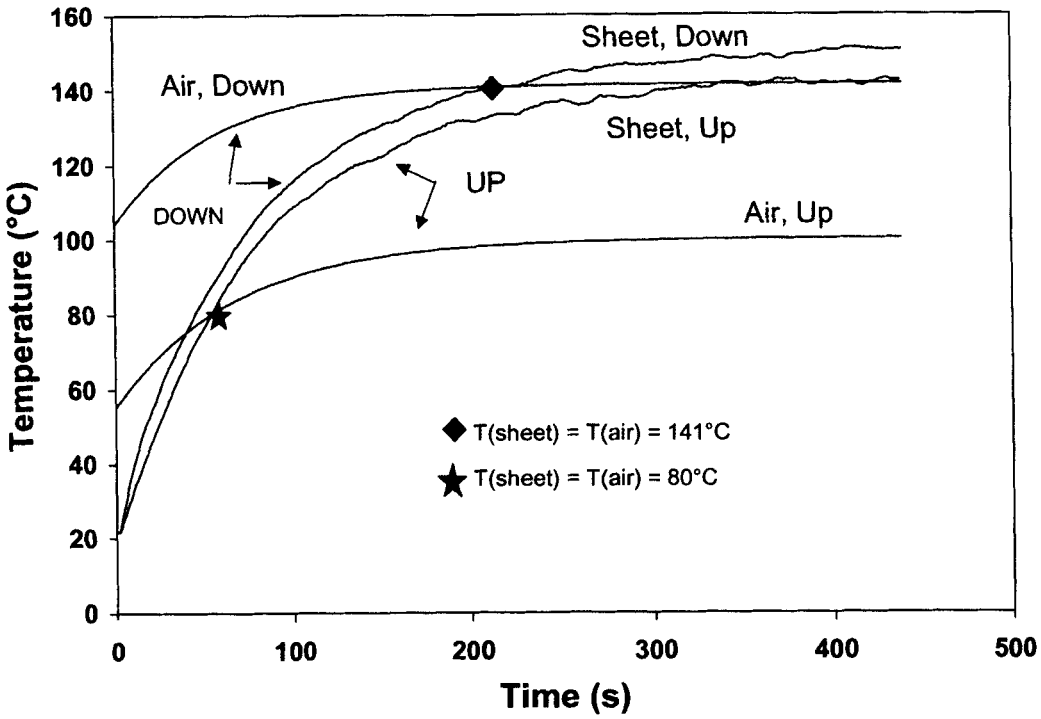

Fig. 11. Sheet surface temperature at the center and midway air temperature measured for the upper and the lower side of the sheet.

reheat phase. Since BF02 heat flux sensors start to heat up at higher temperatures and deviate from their calibration constants, the results at the end of the reheat phase are considered less reliable. The heat flux measurements for the upper side of the sheet failed due to the poor contact between the sensor and the sheet.

To evaluate the natural convective heat transfer coefficient towards the end of the reheat phase, we resorted to empirical equations. *Equations 13* to *15* require the sheet surface temperature as well as the air temperature. *Figure 11* summarizes the required information for the evaluation of the heat transfer coefficient at the center of the sheet. Based on these data, *Figs. 12* and *13* give the heat transfer coefficients for the lower and upper side of the sheet as functions of reheat time, respectively. Both constant and transient air temperatures were considered to allow a later comparison. The discontinuity around 55 s for the upper side and 210 s for the lower side represents the crossover points where the air and sheet surface temperatures coincide (T = 80°C and T = 141°C, see *Fig. 11*). Below these temperatures the empirical equations are not reliable because of the nonuniformity of the air temperature, ranging from sheet surface temperature to oven temperature. Therefore, a comparison cannot be made between the values evaluated using empirical equations for the beginning of the reheat phase with the one obtained using heat flux sensors for the lower side of the sheet. On the other hand, no matter what the air temperature is, the heat transfer coefficient after the crossover point levels off toward the end of reheat phase once the sheet surface temperature reaches equilibrium. The resulting equilibrium value of the heat transfer coefficient for the lower side of the sheet ranges between 2.0 to 3.5 $W.m^{-2}.K^{-1}$. Since the natural convective heat transfer mechanism is different before and after the crossover point, the evaluated values after the crossover point cannot be directly compared to the one measured experimentally for the beginning of the reheat phase. The empirical equations lead to a heat transfer coefficient between 6.5 and 7.5 $W.m^{-2}.K^{-1}$ for the upper side of the sheet regardless of the air temperature, as can be seen in *Fig. 13*. These results imply that the natural convective heat transfer coefficient for the upper side of the sheet is 2–3 times greater than the values obtained for the lower side. This conclusion holds for the majority of conventional thermoforming operations.

Figure 14 shows the variation of the heat transfer coefficient for the upper side of the sheet as a function of the sheet surface temperature. Despite the strong temperature dependency of the heat transfer coefficients, they can be assumed constant for the most of the reheat period due to the slight changes in the sheet surface temperature towards the end of the reheat phase. The evolution of heat transfer coefficients given in *Figs. 12* and *13* also confirms this assumption.

The other parameter investigated in this work was the polymer specific heat. Based on the experimental

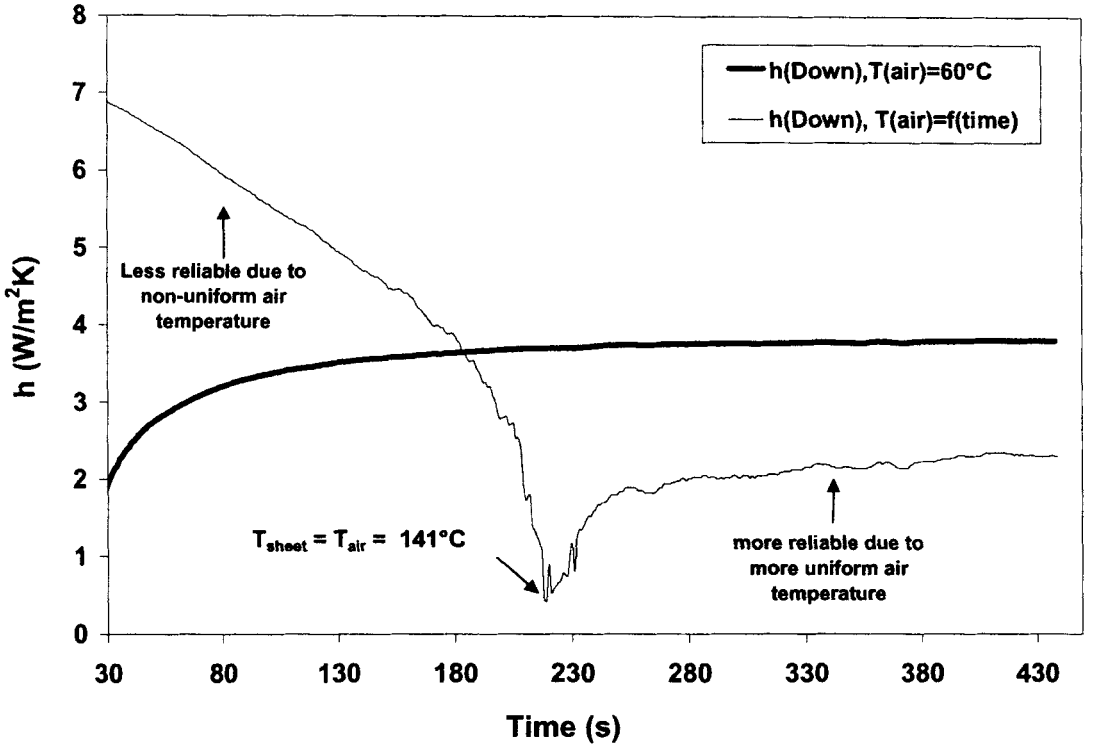

Fig. 12. Transient heat transfer coefficient for the lower side of the sheet evaluated using Eq 15, assuming either constant or transient air temperature.

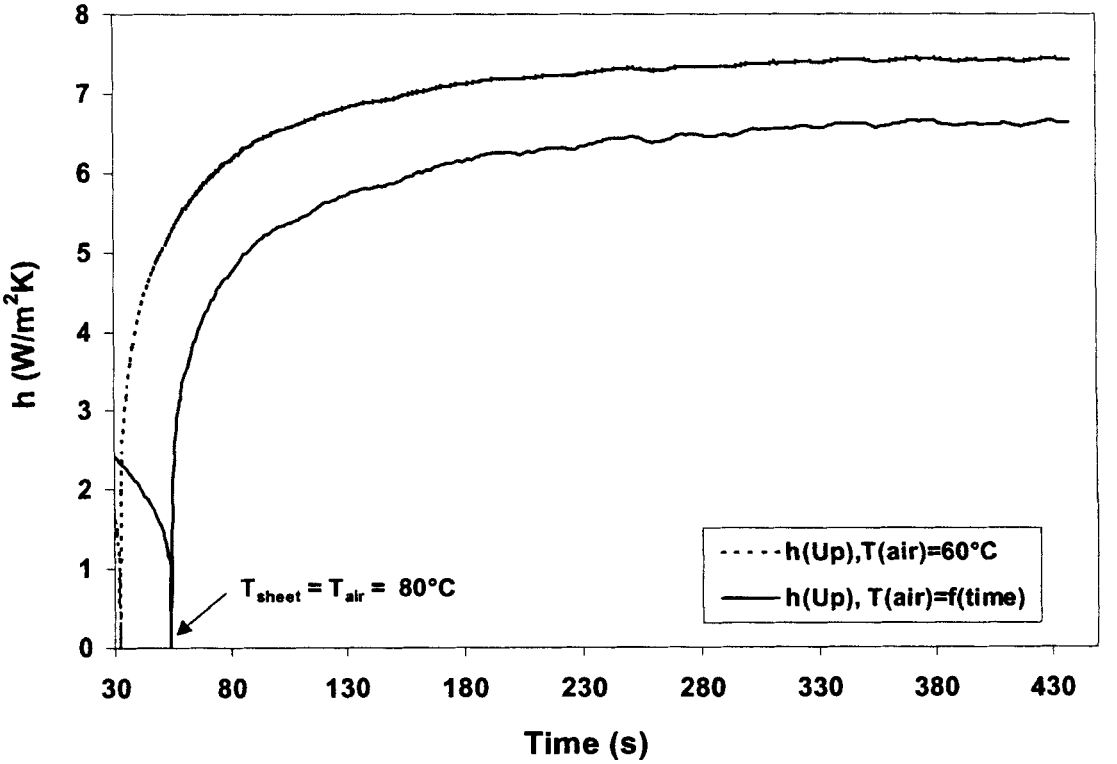

Fig. 13. Transient heat transfer coefficient for the upper side of the sheet evaluated using Eq 13, assuming either constant or transient air temperature.

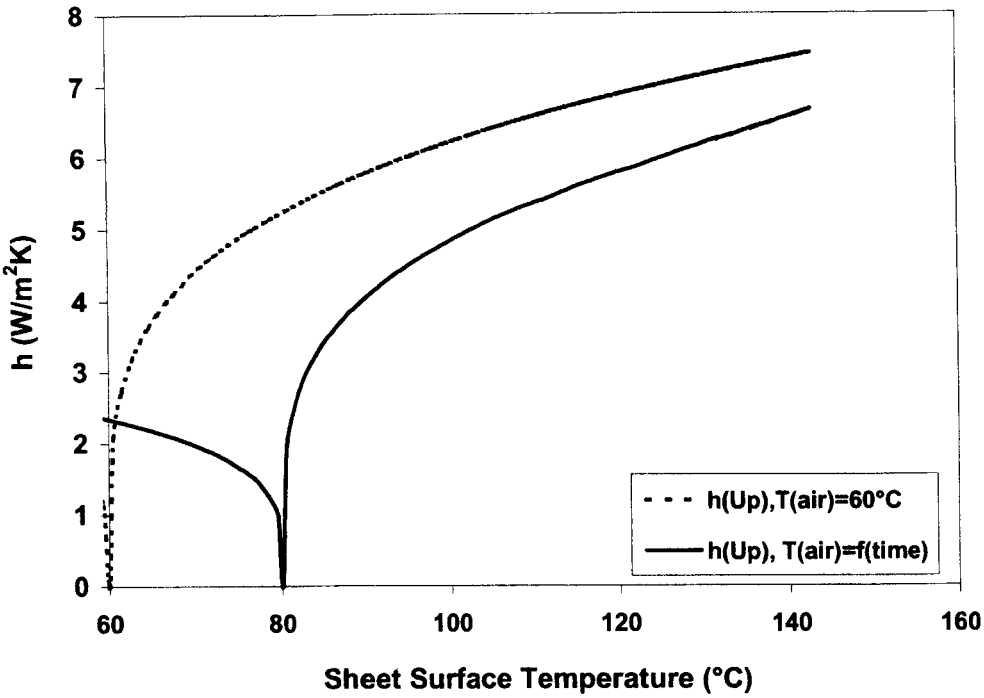

Fig. 14. Heat transfer coefficient for the upper surface of the sheet as a function of temperature evaluated using Eq 13, assuming either constant or transient air temperature.

data taken from the literature, the specific heat was assumed to increase linearly with temperature featuring different slopes below and above glass transition temperature. Differential scanning calorimetry will bring some insight to the magnitude of this parameter for a wide temperature range.

Sheet sag affects the sheet reheat phase through changing the sheet-oven spacing and as a consequence the view factor. In the simulation of the reheat stage, the sag was accounted for through dynamic evaluation of the view factor. *Figure 15* shows how the view factor changes for opposite sides of the sheet as a function of reheat time.

Table 1 summarizes the degree of uncertainty for some of the input parameters. The prediction of sheet reheat phase was improved by implementing appropriate input parameters in the simulations. That is:

1. Measured oven temperatures instead of set points (199°C and 187°C for upper and lower heater banks, respectively).
2. Average air temperatures (60°C for the upper side and 110°C for the lower side of the sheet).
3. Different convective heat transfer coefficients for the upper and lower side of the sheet (7 $W.m^{-2}.K^{-1}$ and 2 to 3 $W.m^{-2}.K^{-1}$, respectively).
4. Measured effective emissivity value of 0.7.
5. Temperature dependent specific heat.
6. Dynamic view factor evaluation.

Figure 16 compares the numerical predictions with experimental measurements for the center of the sheet (lower side) before and after uncertainty treatment. The results indicate that the accuracy of predictions can be significantly improved by accurately evaluating the uncertainty bound for the key parameters through the approach implemented in this work. *Figure 17* gives the thickness prediction results before and after uncertainty treatment as well as the experimental thickness data obtained on a bass boat thermoformed at industrial operating conditions (10). One can also see that the thickness predictions are considerably improved upon the improvement in the prediction of temperature profile prior to forming. These results imply that for various thermoforming operations, proper prediction and treatment of parameter uncertainty for the reheat phase will improve the quality of predictions for the entire process.

CONCLUSION

This work involved the uncertainty treatment, through more accurate measurement of the input parameters. The sensitivity analysis indicated that the sensitivity of the sheet temperature to each processing parameter was dynamic in nature during reheat. The parameter highly affecting the sheet surface temperature was the temperature of the radiant heater. The emissivity of the radiant heater, the view factor, and the polymer specific heat were the other parameters significantly affecting the reheat phase. These results are applicable to a wide range of thermoforming operations

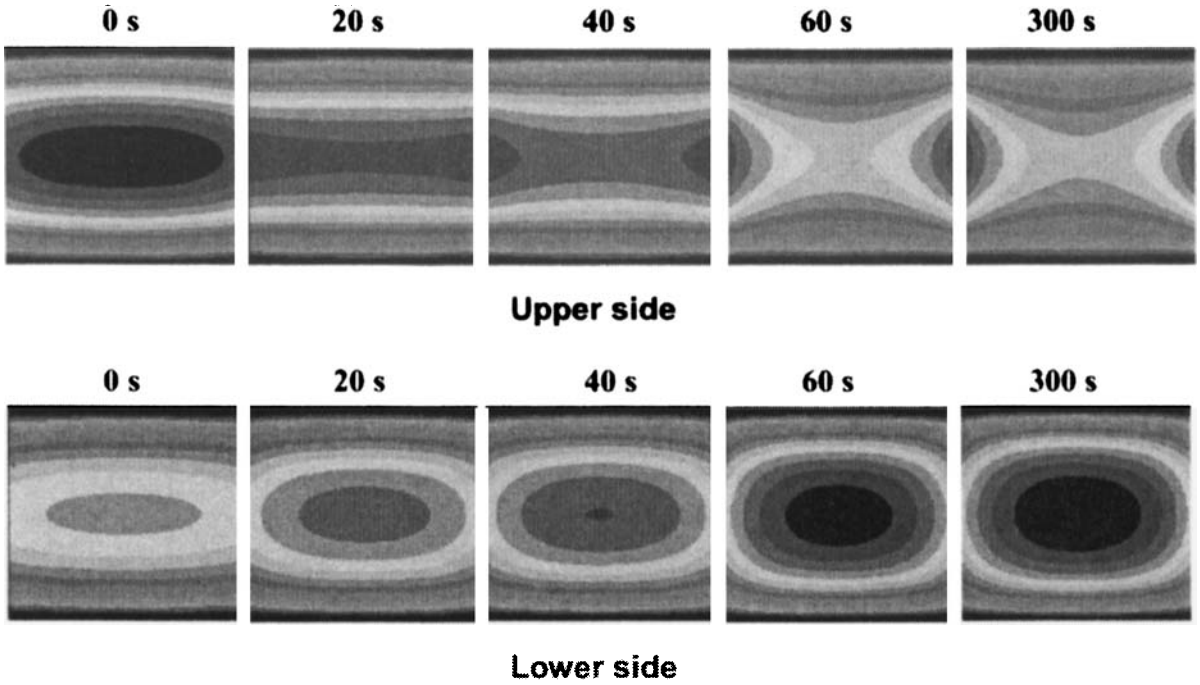

Fig. 15. Variations in the view factor for the upper and the lower side of the sheet as a function of reheat time.

and materials. However, for thick-gauge sheets, the effect of thermal conductivity should be taken into consideration.

The experimental measurements demonstrated a significant discrepancy between the set point and the measured temperature response of the ceramic heaters. Therefore, the heater temperatures input in the simulations must be time dependent to properly predict the reheat stage. An alternative would be to obtain a better transient temperature control of the heating zones. Experimental measurements also demonstrated that the air temperature was extremely nonuniform in all three directions and changed significantly with heating time. Furthermore, the air temperatures at the lower side of the sheet were 1.5 to 2 times greater that the values at the upper side. The heat flux measurements indicated that for the lower surface of the sheet, the heat transfer coefficient is extremely low (2 $W.m^{-2}.K^{-1}$). This was attributed to the clamp frame at the lower side acting as a barrier to the natural heat transfer phenomena by trapping the hot air. Empirical equations lead to a comparable value of the heat transfer coefficient for the lower side of the sheet towards the end of the reheat period. For the upper side of the sheet, heat transfer coefficients approximated by empirical equations were almost three times the value of the lower side.

This work demonstrated that the prediction of sheet reheat phase could be significantly improved by implementing appropriate input parameters in the simulations. That is:

- Measured oven temperatures instead of set-point oven temperatures
- Different air temperatures and convective heat transfer coefficients for the upper and the lower side of the sheet by keeping the respective ratio for each parameter
- Accounting for the geometrical features of the heating elements in evaluation of the effective emissivity
- Temperature-dependent specific heat and dynamic view factor evaluation.

The context of this work is the reheat phase of thermoforming processes and can be generalized for a wide range of equipments, materials and processing conditions. The uncertainty treatment methodology

Table 1. Uncertainty Evaluated for Some Input Parameters.

Parameter	Nominal	Upper bound	Lower bound
Oven temperature (°C)	180	220	170
Air temperature (°C)	60	140	40
Heat transfer coefficient ($W.m^{-2}.K^{-1}$)	5	7.5	2.0
Effective emissivity	0.80	0.95	0.70
Specific heat (J/Kg.K)	1300	2200	800

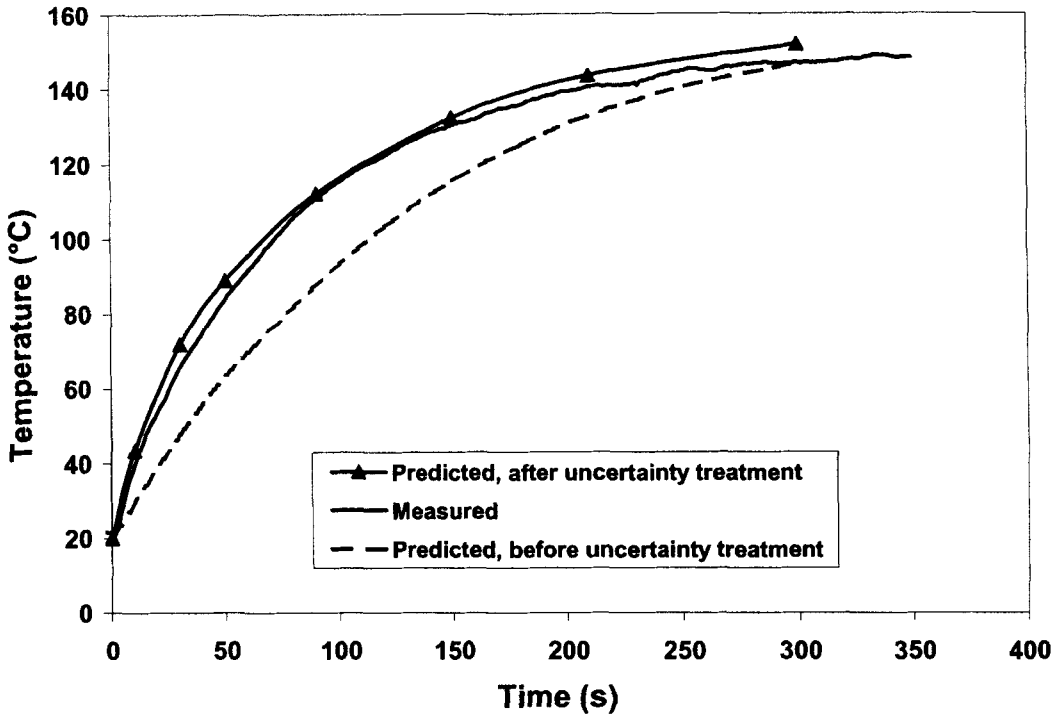

Fig. 16. Improvement in the prediction of sheet reheat phase through the uncertainty treatment.

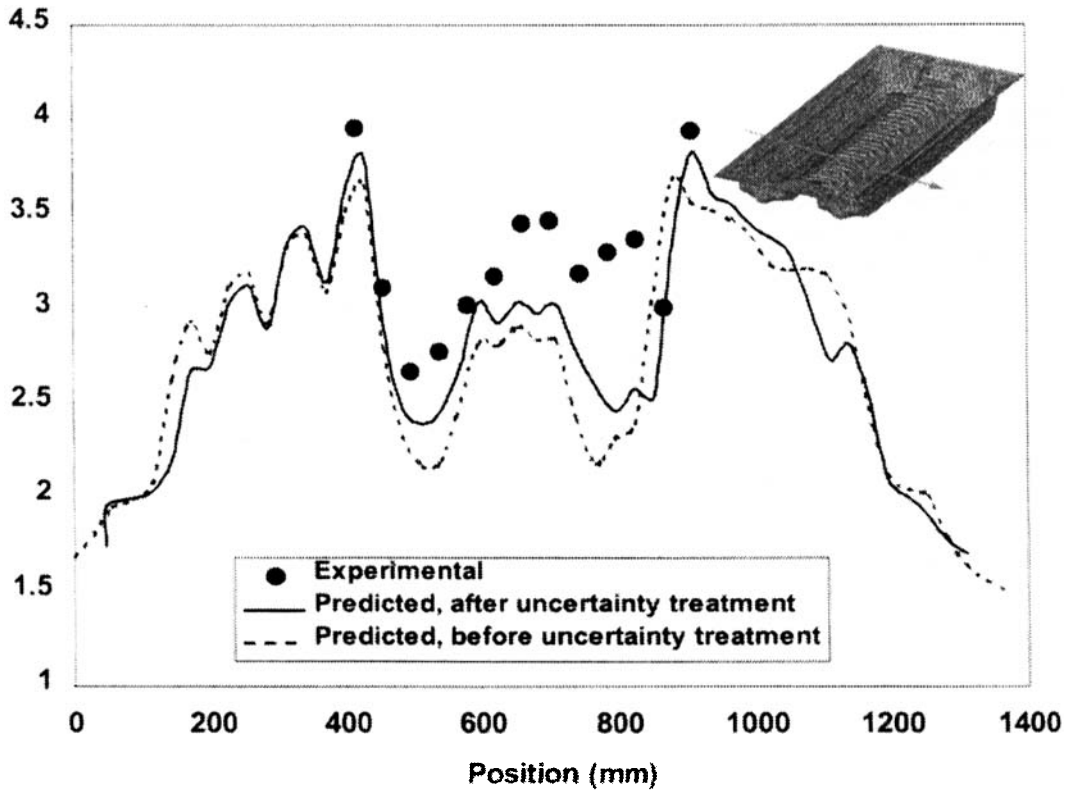

Fig. 17. Improvement in the prediction of thickness profile for a bass boat through the uncertainty treatment. The arrow on the bass boat indicates the location and direction of experimental measurements.

and the observed trends in the processing parameters discussed in this work can directly be applied to improve the accuracy of sheet reheat predictions.

ACKNOWLEDGMENT

The authors would like to acknowledge the valuable technical contributions of Christian De Grandpré, Marc-André Rainville and Denis Laroche in this work.

REFERENCES

1. H. Gross, *Advances in Polymer Technology*, **3**, 233 (1984).
2. J. L. Throne, *SPE ANTEC Tech. Papers*, **35** (1989).
3. J. L. Throne, "Heating Semitransparent Polymers in Thermoforming," *Thermoforming Quarterly*, 7 (1996).
4. F. Schmidt, R. W. DiRaddo, and D. Laroche, *PPS Conference* (1998).
5. S. Monteix, PhD dissertation, Ecole des Mines de Paris (2001).
6. Y. Le Maoult, F. Schmidt, M. El Hafi, and P. Lebaudy, *4th International Workshop on Advanced Infrared Technology and Applications*, 321, Firenze (1997).
7. S. Monteix, F. Schmidt, Y. Lemaoult, R. Ben-Yedder, D. Laroche, and R. DiRaddo, *SPE ANTEC Tech. Papers*, **45** (1999).
8. A. Bendada and K. T. Nguyen, *3rd International Conference on Inverse Problems in Engineering: Theory and Practice* (1999).
9. E. Haberstroh and C. Detrois, Capabilities and Limitations of Injection Stretch Blow Molding Simulation, personal communication, IKV, Germany (1999).
10. D. Laroche and R. Connolly, *SPE ANTEC Tech. Papers*, **46** (2000).
11. M. A. Thrasher, *SPE ANTEC Tech. Papers*, **42** (1996).
12. R. C. Progelhof, J. Quintiere, and J. L. Throne, *J. Applied Polymer Science*, **17**, 1227 (1973).
13. F. M. Duarte and J. A. Covas, *Plastics, Rubber and Composites Processing and Applications*, **26**, 213 (1997).
14. S. Monteix, F. M. Schmidt, Y. Le Maoult, R. Ben Yedder, R. W. DiRaddo, and D. Laroche, Internal Report, Industrial Materials Institute/NRC (1998).
15. R. Ben Yedder and R. Diraddo, Modélisation du chauffage des préformes, Internal Report, Industrial Materials Institute/NRC, Canada (1998).
16. J. L. Throne, *Technology of Thermoforming*, Hanser Publishers (1996).
17. R. DiRaddo, D. Laroche, A. Bendada, and T. Ots, *SPE ANTEC Tech. Papers*, **44** (1998).
18. B. Bernstein *et al.*, *Trans. Soc. Rheol.*, **7**, 391 (1963).
19. F. P. Incropera and D. P. De Witt, *Introduction to Heat Transfer*, John Wiley & Sons (1985).
20. D. Laroche and R. DiRaddo, "Computer Technologies for Modelling and Optimization of the Blow Moulding Process," chapter in *Blow Moulding Handbook*, N. Lee, ed., Chapman and Hall Publishers (in press 2001).
21. P. Debergue and D. Laroche, *SPI Conference* (2000).
22. A. Yousefi, A. Bendada, and R. DiRaddo, *SPE ANTEC Tech. Papers*, **46** (2000).